Bionanocomposites from Renewable Resources: Epoxidized Linseed Oil−Polyhedral Oligomeric Silsesquioxanes Hybrid Materials

Gerard Lligadas, Joan C. Ronda, Marina Galià,* and Virginia Cádiz

Departament de Química Analítica i Química Orgànica, Universitat Rovira i Virgili, Campus Sescelades, Marcel.lí Domingo s/n, 43007 Tarragona, Spain

Received July 19, 2006; Revised Manuscript Received September 22, 2006

This study is concerned with the preparation and properties of a new class of bionanocomposites from renewable resources. Epoxidized linseed oil (ELO) and 3-glycidylpropylheptaisobutyl-T_8-polyhedral oligomeric silsesquioxane (G-POSS) (2, 5, and 10 wt %) were cross-linked, and Fourier transform infrared spectroscopy (FTIR), dynamic mechanical thermal analysis (DMTA), thermogravimetric analysis (TGA), and scanning electron microscopy (SEM) were employed to characterize the POSS-reinforced oil-based polymer networks. No POSS aggregates were observed for the 2 wt % G-POSS nanocomposite by SEM. POSS-rich particles with diameters of several nanometers were observed in the nanocomposites with 5 and 10 wt % G-POSS. Enhanced glass transition temperatures and storage moduli of the networks in the glassy state and rubber plateau were observed to be higher than those of the POSS-free oil based polymer network, due to the reinforcement effect of POSS cages.

Introduction

Growing interest in the exploitation of renewable resources in the areas of energy and materials has been one of the major scientific and technological issues of these past few decades. Vegetable oils represent one of the cheapest and most abundant biological feedstocks available in large quantities, and their use as starting materials offers numerous advantages, such as low toxicity and inherent biodegradability.[1] Although they possess double bonds, which are used as reactive sites in coatings, they can also be functionalized by epoxidation. Epoxidized vegetable oils show excellent promise as inexpensive, renewable materials for industrial applications.[2] In recent years, extensive work has been done to develop polymers from epoxidized triglycerides or fatty acids.[3] The cationic polymerization of epoxidized vegetable oils has been investigated using photoinitiated[4] and thermal[5] latent cationic catalysts to produce biobased epoxy resins with promising properties. Latent initiators show no activity under normal conditions, but form active species to initiate polymerization only with external stimuli such as heating or photoirradiation.[6]

Triglycerides are made up of aliphatic chains, and, consequently, the triglyceride-based materials are incapable of the necessary rigidity and strength required for some applications.[7] There has been great interest in organic−inorganic hybrid materials because of their unusual properties, derived from unique combinations of each component.[8] Specifically, the physical, mechanical, and thermal properties may be greatly improved. Regarding vegetable oil-based hybrid materials, composites with good mechanical properties have been prepared from acrylate-modified soybean oil and natural fibers,[9] organic−inorganic hybrid coatings have been developed using plant oils and metal (Ti and Zr) oxides,[10] organic−inorganic hybrid networks with good transparency were developed by hydrosilylation of alquenil-terminated fatty acid derivatives,[11] and carbon nanotubes have been used as reinforcements for acrylated epoxidized soy oil resins.[12] In addition, a new class of green hybrid materials incorporating clay[13−15] or a silica network[16] into a vegetable oil polymer matrix has been reported.

Polymers reinforced with well-defined nanosized inorganic clusters have attracted a tremendous amount of interest because of their versatility; among these systems, polyhedral oligomeric silsesquioxane (POSS) compounds, which possess a unique cagelike structure and nanoscale dimensions, are of particular interest. POSS compounds are 1−3 nm in diameter, and their inorganic cage framework is made up of a fixed proportion of silicon and oxygen: $(SiO_{1.5})_n$, where $n = 8$, 10, or 12. Different polymerizable POSS macromers have been employed to copolymerize with organic monomers, via the formation of covalent bonds, to afford a variety of polymer/POSS nanocomposites.[17] Epoxy resins/POSS nanocomposites are the most studied of these nanocomposites, and various mono-[18,19] or polyepoxide[20] POSS monomers have been used to modify epoxy networks. The incorporation of POSS derivatives into polymeric materials can lead to substantial improvements in polymer properties including increases in use temperature[21] and mechanical properties,[22] as well as reductions in flammability,[23] heat evolution,[24] and viscosity[25] during processing. These property improvements have encouraged academic and industrial research, which were critical in both reducing the prices and increasing production of POSS feedstocks.

To the best of our knowledge, this is the first example of the preparation of biobased POSS nanocomposites from plant oil derivatives. In this study, 3-glycidylpropylheptaisobutyl-T_8-polyhedral oligomeric silsesquioxane (G-POSS, Chart 1) was incorporated into an epoxidized linseed oil (ELO, Chart 1) cross-linked network, by cationic-initiated polymerization. The cationic latent initiator used in this study was *N*-benzylpyrazinium hexafluoroantimoniate (BPH, Chart 1). Chemical incorporation of G-POSS into the network was studied by solvent extraction and Fourier transform infrared (FTIR) analysis; the morphology of these nanocomposites was determined by X-ray diffraction (XRD) and scanning electron microscopy (SEM); and the nanoscale reinforcement effect of POSS on the prepared epoxy

* Corresponding author. E-mail: marina.galia@urv.cat.

10.1021/bm060703u CCC: $33.50 © 2006 American Chemical Society
Published on Web 11/11/2006

Chart 1. Chemical Structure of Epoxidized Linseed Oil (ELO), 3-Glycidylpropylheptaisobutyl-T_8-polyhedral Oligomeric Silsesquioxane (G-POSS), and *N*-Benzylpyrazinium Hexafluoroantimoniate

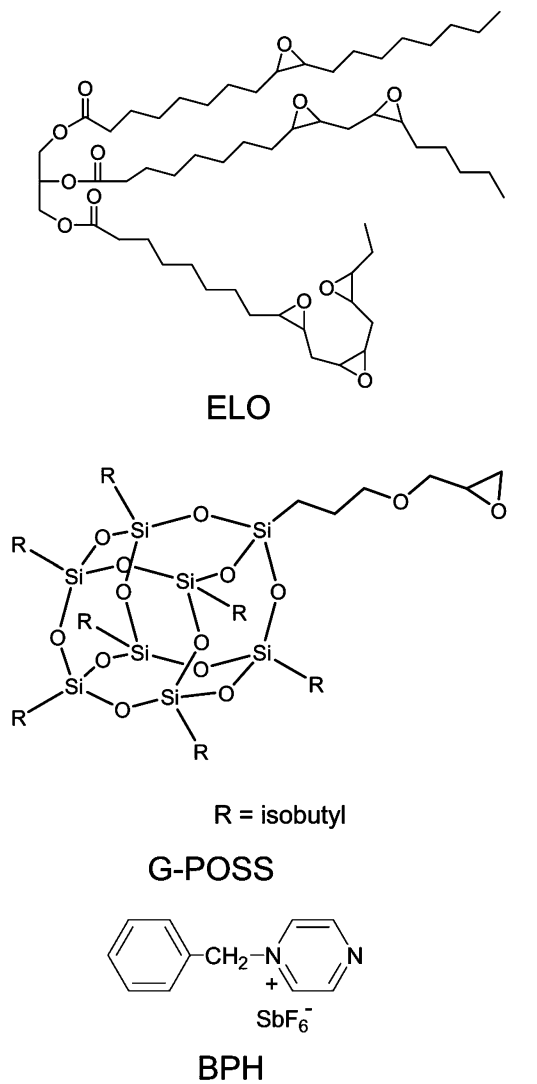

biobased nanocomposites was evaluated using differential scanning calorimetry (DSC), dynamic mechanical thermal analysis (DMTA), and thermogravimetric analysis (TGA).

Experimental Section

Materials. The linseed oil and 3-glycidylpropylheptaisobutyl-T_8-polyhedral oligomeric silsesquioxane (G-POSS, Chart 1) used in this study were supplied by Aldrich and were used as received. The following chemicals were obtained from the sources indicated, formic acid (Scharlau), hydrogen peroxide 50% w/v (Aldrich), sodium hexafluoroantimoniate (Aldrich), pyrazine (Aldrich), benzyl bromide (Fluka), and all were used without further purification. All solvents were purified by standard procedures.

N-Benzylpyrazinium hexafluoroantimoniate (BPH) was synthesized in our laboratory according to the published procedure.[6]

Epoxidation of Linseed Oil. A solution of linseed oil (20.1 g, 67.0 mmol) and formic acid (1.0 mL, 26.2 mmol) was stirred at 45 °C, and H_2O_2 50% w/v (38 mL, 659.0 mmol) was added dropwise. After H_2O_2 addition was complete, the temperature was raised to 70 °C and the flask contents were stirred vigorously for 6 h. The mixture was then cooled and transferred to a separating funnel containing ethyl acetate (75 mL). The organic fraction was washed with approximately 100 mL of distilled water and 100 mL of saturated sodium bicarbonate solution (aqueous). These washings were continued until the pH reached 7. The ethyl acetate solution was then dried over anhydrous magnesium sulfate, filtered, and concentrated in vacuo to give the product as a clear oil with a yield of 96%.

FTIR (cm^{-1}): 2957, 2860 (ν, C−H), 1743 (ν, C═O), 825 (ν, C−O oxirane ring).

^{1}H NMR ($CDCl_3$): δ = 0.8−1.1 (−CH_3 of fatty acids), 1.2−1.8 (−CH_2− of fatty acids), 2.3 (−CH_2C═O−), 2.8−3.2 (−CH−O−CH−), 4.1−4.3 (CH_2−O−C═O), 5.2 (−CH−O−C═O).

^{13}C NMR ($CDCl_3$): δ = 10.6, 14.2 (−CH_3 of fatty acids), 21.2−34.8 (−CH_2− of fatty acids), 54.1−58.0 (−CH−O−CH−), 62.2 (−CH_2−O−C═O), 68.9 (CH−O−C═O), 172.4, 172.7, 172.8 (C═O).

General Preparation of ELO/G-POSS Bionanocomposites. To prepare the bionanocomposites containing POSS (2, 5, and 10 wt %), the desired amount of G-POSS was dissolved in a minimum of acetone, and this solution was added to preweighted ELO. On formation of a homogeneous solution, 1 wt % of the latent catalyst (BPH) was added. The mixture was stirred for 2 h, and the solvent was removed under vacuum. The mixture was cast and cured in a mold at 140 °C for 1 h, 170 °C for 2 h, and 190 °C for 1 h, in air using an oven. The curing conditions were determined from the DSC data. ELO homopolymer was prepared under the same curing conditions for comparison. Ground to powder samples (∼1.0 g) of every nanocomposite were immersed into a large excess of tetrahydrofuran or chloroform and refluxed for 12 h to determine if any soluble material could be extracted by the solvent.

Measurement and Techniques. The FTIR spectra were recorded on a Bomem Michelson MB 100 FTIR spectrophotometer with a resolution of 4 cm^{-1} in the absorbance mode. An attenuated-total-reflection (ATR) accessory with thermal control and a diamond crystal (Golden Gate heated single-reflection diamond ATR, Specac-Teknokroma) was used to determine FTIR spectra.

The NMR spectra were recorded on a Varian Gemini 400-MHz spectrometer (400 MHz for ^{1}H, 100.57 MHz for ^{13}C). The samples were dissolved in deuterated chloroform, and spectra were obtained at room temperature using TMS as an internal standard.

Calorimetric studies were carried out on a Mettler DSC822e thermal analyzer in a dry nitrogen atmosphere. All of the samples (about 10 mg in weight) were heated from −80 to 150 °C at a rate of 20 °C/min.

Thermal stability studies were carried out on a Mettler TGA/SDTA851e/LF/1100. The samples (about 10 mg) were heated, under nitrogen or air atmospheres, from ambient temperature to 800 °C at a rate of 10 °C/min.

Dynamic mechanical properties were measured with a dynamic mechanical thermal analyzer (DMTA) (TA DMA 2928). Specimens with dimensions 2 mm × 5 mm × 10 mm were tested in a three-point bending configuration. The various thermal transitions were studied between −80 and 90 °C at a heating rate of 5 °C/min and at a fixed frequency of 1 Hz.

WAXD measurements were made using a Siemens D5000 diffractometer (Bragg-Brentano parafocusing geometry and vertical $\theta-\theta$ goniometer) fitted with a curved graphite diffracted-beam monochromator, incident and diffracted-beam Soller slits, a 0.06° receiving slit, and scintillation counter as a detector. The angular 2θ diffraction range was between 1° and 40°. Samples were dusted onto a low background Si(510) sample holder. The data were collected with an angular step of 0.05° at 3 s per step. Cu K_α radiation was obtained from a copper X-ray tube operated at 40 kV and 30 mA.

The surfaces of different biobased nanocomposites were observed with SEM. A gold coating, which is a few nanometers thick, was made on the fracture surfaces to be observed. A JEOL JSM 6400 SEM with a field emission filament and an accelerating voltage of 10 kV was used to collect SEM images for all samples. For the atomic mapping, an Oxford INCA energy-dispersive X-ray Micro Analyzer was used.

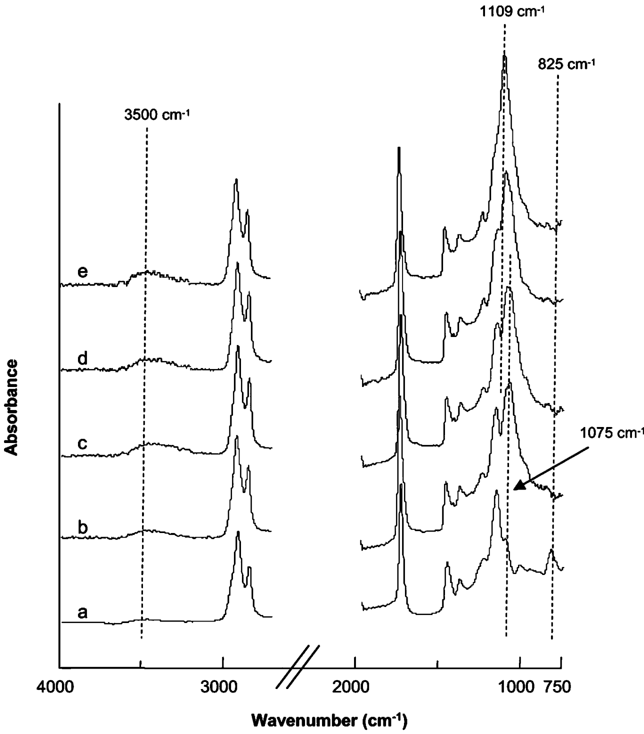

Figure 1. FTIR spectra of ELO (a), ELO polymer (b), and ELO nanocomposites containing G-POSS: 2 wt % (c), 5 wt % (d), and 10 wt % (e).

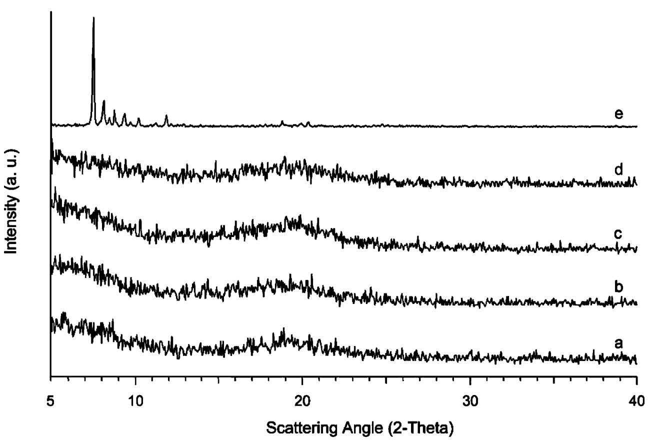

Figure 2. WAXD data of ELO polymer (a), ELO nanocomposites containing G-POSS: 2 wt % (b), 5 wt % (c), 10 wt % (d), and G-POSS (e).

Results and Discussion

In this study, epoxidized linseed oil (ELO, Chart 1) and 3-glycidylpropylheptaisobutyl-T_8-polyhedral oligomeric silsesquioxane (G-POSS, Chart 1) were used as organic monomers and inorganic nanoparticules, respectively. Naturally linseed oil contains triglycerides consisting of a mixture of linolenic (57%), oleic (19%), linoleic (15%), palmitic (5%), and stearic (4%) fatty acids. ELO was prepared by the reaction of linseed oil with formic acid and hydrogen peroxide at 70 °C for 6 h. The chemistry of the Prileshajev epoxidation of unsaturated fatty compounds is well known:[26] a short-chain peroxy-acid is prepared from hydrogen peroxide and the corresponding acid, either in a separate step or in situ.[27] The structure of ELO was confirmed by its FTIR, and ^{1}H and ^{13}C NMR spectra. The epoxy group number of ELO per molecule, determined by ^{1}H NMR spectroscopy, was 5.6.

The bionanocomposites were synthesized by curing the epoxidized linseed oil and the designated amount of G-POSS, using 1 wt % of *N*-benzylpyrazinium hexafluoroantimoniate (BPH, Chart 1) as a thermally latent cationic catalyst on the basis of published results.[5] The C−N bond in BPH is thermally cleaved to generate a benzyl cationic reactive species, which catalyzes the cationic polymerization of the epoxides.[6] ELO nanocomposites containing 2, 5, and 10 wt % of G-POSS and neat ELO polymer were prepared by thermal curing at 140 °C for 1 h, 170 °C for 2 h, and 190 °C for 1 h (conditions determined by DSC).

All of the cured nanocomposites were homogeneous and transparent, implying that no phase separation had occurred, at least on the scale greater than the wavelength of visible light. All samples were refluxed in chloroform or tetrahydrofuran (THF) for 12 h to dissolve and extract any soluble components present. No soluble fractions were detected in the solvent residues, suggesting that the cross-linking reaction had occurred between the two components and showing that all of the cured composites were no longer soluble. FTIR spectra of the above POSS-containing nanocomposites allowed examination of the degree of curing after the introduction of POSS into the network. Shown in Figure 1 are the FTIR spectra of ELO, the ELO polymer, and the hybrid composites containing 2, 5, and 10 wt % POSS. ELO is characterized by the stretching vibration of the epoxide moieties at 825 cm^{-1} (C−O−C), and completion of the curing reaction was confirmed by its complete disappearance (see curves b−e). New bands were also observed at 1075 and 3500 cm^{-1} and were assigned to the aliphatic ether and terminal hydroxyl groups produced during oxirane ring opening. The absorption at 1109 cm^{-1}, assigned to Si−O−Si of the POSS, is present in all of the composites and indicates a silsesquioxane structure, its intensity increasing with POSS concentration.

The morphology of the POSS bionanocomposites was further investigated by wide-angle X-ray diffraction (WAXD), energy-dispersive X-ray spectroscopy (EDX) Si-mapping, and scanning electron microscopy (SEM). The WAXD patterns of the nanocomposites are shown in Figure 2; for comparison, the X-ray patterns of G-POSS and the neat ELO polymer are also shown. The diffractogram of the G-POSS shows a main reflection at 2θ of 7.4° and a series of smaller peaks at 2θ's of 8.1°, 8.7°, 9.3°, etc. This complicated diffractogram and the presence of two well-defined melting peaks, at 112 and 132 °C, in the DSC thermogram may indicate the coexistence of two different crystalline phases. The WAXD patterns of all of the ELO nanocomposites are similar to that of the neat ELO polymer, displaying a broad peak with 2θ around 20°, corresponding to an amorphous halo. Therefore, the WAXD data give no indication of the presence of crystalline POSS aggregate in the synthesized nanocomposites. However, because of the limited sensitivity of WAXD, the occurrence of some clustering of POSS units or phase-separated small-sized inorganic domains cannot be ruled out.

The homogeneity of the POSS nanoparticules dispersion was further examined with SEM. As a first approach, EDX Si-mapping of all of the composites showed that the particles were uniformly dispersed in the cross-sectional surfaces observed (Figure 3). The white points in the image denote POSS-enriched regions. Figure 4 displays the SEM cross-sectional images of ELO/G-POSS composites having different POSS contents. The SEM micrograph of the composite containing 2 wt % G-POSS exhibits a featureless morphology, with no discernible phase separation, suggesting that POSS nanoparticles are homogeneously dispersed throughout the matrix. When the concentration of POSS was 5 wt %, the SEM micrograph reveals aggregation,

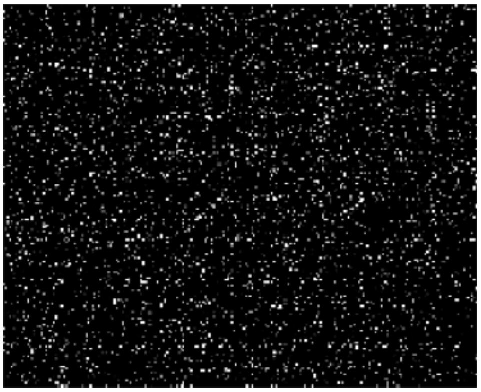

Figure 3. SEM-EDX Si-mapping micrograph of a cross section of ELO 5 wt % G-POSS nanocomposite.

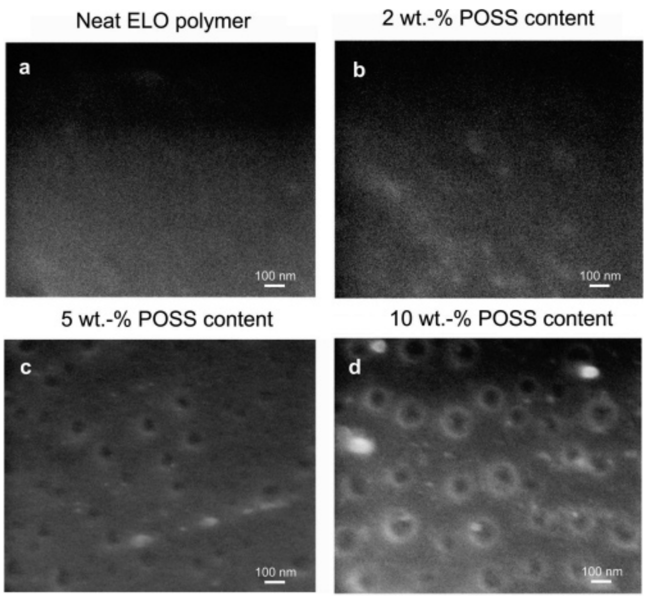

Figure 4. SEM cross-sectional micrographs of ELO polymer (a) and ELO nanocomposites containing G-POSS: 2 wt % (b), 5 wt % (c), and 10 wt % (d).

showing many spherical particles (40−50 nm in diameter) uniformly dispersed. More serious aggregation (80−150 nm in diameter) occurs in 10 wt % containing composite. This behavior can be explained assuming that the reactivity of epoxy POSS is likely to be lower as compared to that of ELO due to steric hindrance; phase separation of G-POSS rich domains could occur at low conversions, before a significant advance in the copolymerization with ELO occurs. G-POSS, which is initially soluble in the monomer mixture, phase separates because its solubility in the organic medium becomes lower during the polymerization, and this phase separation occurs at lower conversions when increasing G-POSS content. These particles may contain ELO segments chemically bonded, in agreement with the reduced crystallinity.

The thermal behavior of ELO/POSS bionanocomposites was investigated by DSC and DMTA. All of the DSC thermograms display single glass transition temperatures (Tg's) in the experimental temperature range, attributed to the ELO matrices. Although the SEM micrograph of 10 wt % G-POSS containing composite showed a heterogeneous morphological structure, no separated Tg values were detected. The approximate Tg values, determined by DSC, are listed in Table 1. The transition was broad, and therefore greater accuracy was not possible. Using DMTA, it was possible to determine with far greater accuracy the Tg of the cross-linked materials: it is measured at the

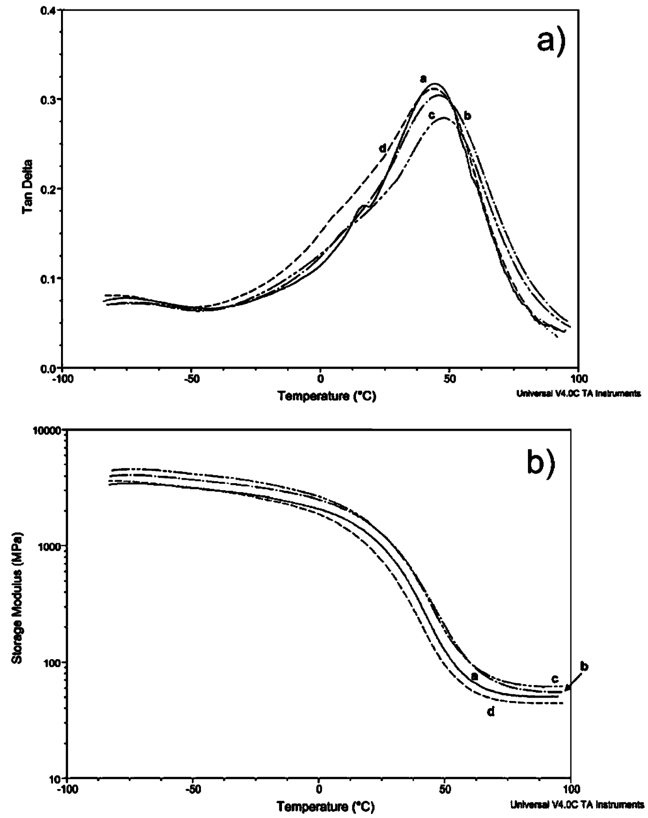

Figure 5. (a) DMTA tan δ and (b) DMTA dynamic storage moduli (E') plots as a function of temperature for the neat ELO polymer (a) and ELO nanocomposites containing G-POSS: 2 wt % (b), 5 wt % (c), and 10 wt % (d).

maximum intensity of the tan δ curves, which reflects the viscous-elastic characteristic of a polymeric material. Shown in Figure 5a are the DMTA plots of tan δ as a function of temperature for the ELO polymer and its nanocomposites. The neat ELO polymer exhibits a well-defined α relaxation peak centered at 44 °C, which corresponds to the glass transition of the polymer. The ELO/POSS nanocomposites that contain 2, 5, and 10 wt % of G-POSS also clearly exhibit a single transition at 49, 52, and 42 °C, respectively. The glass transition behavior of the nanocomposite systems is dependent on the morphology of the hybrid composites. The Tg of the nanocomposites slightly increased and the intensity of the α transition decreased with an increasing POSS content up to 5 wt %. This observation is ascribed to the nanoreinforcement effect of the POSS cages on oil-based polyether networks.[19] The bulky POSS cages may restrict the motion of the macromolecular chains, and thus higher temperatures are required to provide the requisite thermal energy to cause a glass transition in hybrid materials. However, the Tg of the composite that contains 10 wt % G-POSS does not follow the same trend. The decreased Tg for this phase-separated composite could be attributed to the incomplete curing reaction due to the inclusion of bulky POSS cages. Infrared spectroscopy (Figure 1) showed the disappearance of the epoxide band at 825 cm^{-1}, suggesting that the curing reaction occurred to completion. The glass transition behavior cannot be explained solely on the basis of the nanoreinforcement effect. The depression of Tg could be ascribed to the increase in free volume of the system due to the inclusion of bulky POSS cages and the lower cross-linking density in the composite. The tan δ plots for all samples displayed a β relaxation at approximately −60 °C. This β transition, which is generally observed in fatty acid

Table 1. Thermal Properties of ELO/G-POSS Nanocomposites

				TGA (nitrogen)		TGA (air)	
entry	ELO/G-POSS wt %	Tg[a] (DSC)	Tg[b] (DMTA)	$T_{5\%loss}$ (°C)[c]	$R_{800°C}$ (%)[d]	$T_{5\%loss}$ (°C)[c]	$R_{800°C}$ (%)[d]
1	100:0	29	44	357	3	327	0
2	98:2	35	49	355	4	338	2
3	95:5	39	52	356	5	334	4
4	90:10	30	42	355	5	327	7

[a] Rough estimation from a broad transition. [b] Maximum of tan δ. [c] Temperature of 5% of weight loss. [d] Char yield at 800 °C.

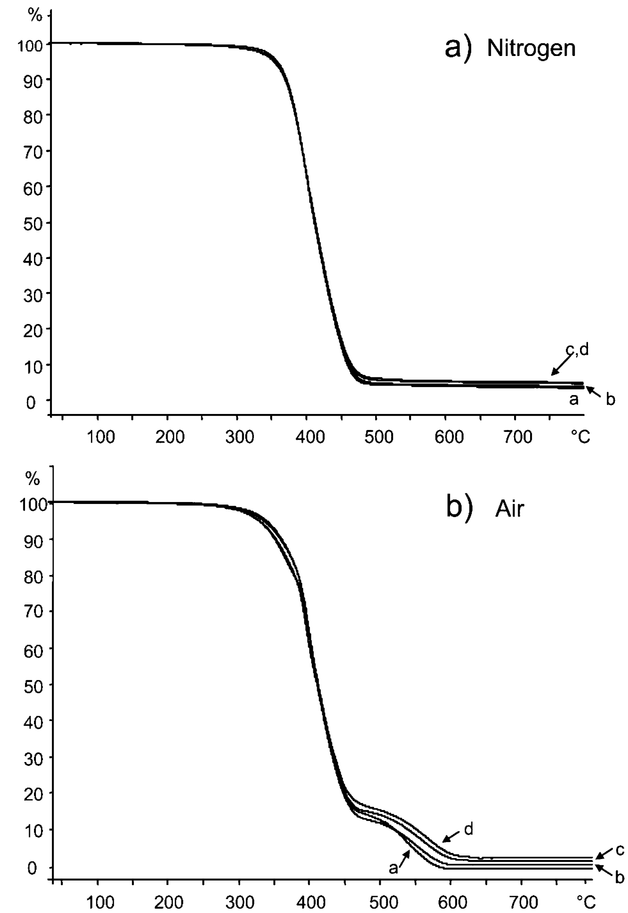

Figure 6. TGA thermograms for the neat ELO polymer (a) and ELO nanocomposites containing G-POSS: 2 wt % (b), 5 wt % (c), and 10 wt % (d) under (a) nitrogen and (b) air atmospheres.

containing thermosets, may be related to the rotational motions of short units in the fatty acid chain.[28]

Figure 5b shows the dynamic storage moduli (E') as a function of temperature for neat ELO polymer and all of its composites. All materials exhibit E' curves with the typical behavior of cross-linked polymeric networks. At low temperature, there is a glassy state with E' staying at a high moduli plateau and a rubbery state with a lower E' for temperatures higher than Tg. As can be seen in Figure 5b, at −80 °C the E' of the hybrids is slightly higher than E' of the neat ELO polymer; therefore, the introduction of small amounts of POSS cages gave rise to a small increase in E' in the glassy state. It is also worth noticing that the E' at the rubbery plateau for POSS-containing polymers was close to or higher than that of the neat ELO polymer. Only at the higher concentration of G-POSS was the storage modulus in the rubbery plateau lower than that of the neat ELO polymer. This behavior has been observed by other authors[29] and can be related to the nanoreinforcement effect of the POSS cages on the netwoks that will give an increase in E' in the glassy and the rubbery states. The inclusion of POSS could give a decrease in the densities of the materials ascribed to an increase in the free volume of the nanocomposites that can come from the increase in the free volume caused by the interaction of POSS cages and polymer chains, and also from the nanoporosity of the POSS core. The cross-linking density per unit volume will decrease with increasing concentration of the POSS in the hybrids, which will result in a decrease in E' of the nanocomposites. Nonetheless, it can be seen that the storage moduli of the hybrids with less than 10 wt % of G-POSS are higher than that of the neat oil network. This implies significant nanoreinforcement by the POSS cages, which counteracts the effect of decreased densities on the storage moduli. Only at higher POSS contents could the effect of the reduced density dominate over the nanoreinforcement effect.[30]

Thermogravimetric analysis (TGA) was used to evaluate the thermal stability of these composites as a function of the POSS content. Table 1 collects the TGA data determined under nitrogen and air atmospheres, and Figure 6a shows the TGA curves for all samples under nitrogen atmosphere at 10 °C/min. For all samples, there is only a single degradation process under nitrogen, which is due to the degradation of the cross-linked polymer network, suggesting that the presence of POSS does not significantly alter the degradation mechanism of the ELO polymers. For the POSS-containing polymers, the char yields at 800 °C slightly increased with the POSS content. The TGA experiments were also carried out in the presence of air as the carrier gas. Under air, a second step in the weight loss rate appears at higher temperature, above 450 °C, corresponding to the thermo-oxidative degradation. Figure 6b shows that under air atmosphere hybrids with POSS content up to 5 wt % are more thermally stable than the neat ELO polymer. It has been proposed that the tethering of the structure of the POSS cage to the organic polymer was crucial to improve the thermal stabilities of POSS-containing nanocomposites.[31] The temperature of 5% of weight loss ($T_{5\%loss}$) is slightly increased because the POSS cages retard the movement of the molecular chains at high temperature (see Table 1). The aggregated structure when POSS content is at 10 wt % reduces its overall effectiveness in hindering polymer movement and its Td value. It is noted that the char residues under air atmosphere increase with POSS content and are in good agreement with the added POSS, which would be converted into inorganic silica at high temperatures. High char yields correspond to reduced amount of volatile and combustible compounds evolving from the thermal degradation processes and improved flammability.

Conclusions

In conclusion, new biobased nanocomposites have been developed from plant oils as renewable resources. The bionanocomposites were obtained from epoxidized linseed oil and 3-glycidylpropylheptaisobutyl-T_8-polyhedral oligomeric silsesquioxane. Most of the resulting POSS-containing networks displayed slightly enhanced glass transition temperatures. The storage moduli of the networks at the glassy and the rubbey plateau were observed to be somewhat higher than that of the POSS-free network. These results can be ascribed to the nanoscale reinforcement effect of POSS cages on the cross-linked matrix.

Acknowledgment. We gratefully acknowledge the CICYT (Comisión Interministerial de Ciencia y Tecnología) (MAT2005-01593) for financial support for this work and the DURSI (Departament d'Universitats, Recerca i Societat de la Informació) and Fons Social Europeu for G.L's predoctoral (2003FI00765) grant. We would like to thank F. Guirado for XRD and M. Moncusí for SEM analysis.

References and Notes

(1) Baumann, H.; Bühler, M.; Fochem, H.; Hisrsinger, F.; Zoeblein, H.; Falbe, J. *Angew. Chem., Int. Ed. Engl.* **1988**, *27*, 41. Biermann, U.; Friedt, W.; Lang, S.; Lühs, W.; Machmüller, G.; Metzger, J. O.; Klaas, M. R.; Schäfer, H. J.; Schneiderüsch, M. P. *Angew. Chem., Int. Ed.* **2000**, *39*, 2206. Eissen, M.; Metzger, J. O.; Schmidt, E.; Schneidewind, U. *Angew. Chem., Int. Ed.* **2002**, *41*, 414.

(2) Kaplan, D. L. *Biopolymers from Renewable Resources*; Springer: Berlin, 1998; p 267.

(3) Lligadas, G.; Ronda, J. C.; Galià, M.; Cádiz, V. *Biomacromolecules* **2006**, *7*, 2420. Lligadas, G.; Ronda, J. C.; Galià, M.; Biermann, U.; Metzger, J. O. *J. Polym. Sci., Part A: Polym. Chem.* **2006**, *44*, 634. Pelletier, H.; Belgacem, N.; Gandini, A. *J. Appl. Polym. Sci.* **2006**, *99*, 3218. Uyama, H.; Kuwabara, M.; Tsujimoto, T.; Kobayashi, S. *Biomacromolecules* **2003**, *4*, 211. Esen, H.; Kusefoglu, S. H. *J. Appl. Polym. Sci.* **2003**, *89*, 3882. Bunker, S. P.; Wool, R. P. *J. Polym. Sci., Part A: Polym. Chem.* **2002**, *40*, 451. Petrovic, Z.; Guo, A.; Zhang, W. *J. Polym. Sci., Part A: Polym. Chem.* **2000**, *38*, 4062. Petrovic, Z.; Guo, A.; Javni, I. U.S. Patent 6,107,433, 2000.

(4) Crivello, J. V.; Narayan, R. *Chem. Mater.* **1992**, *4*, 692.

(5) Park, S. J.; Jin, F. L.; Lee, J. R.; Shin, J. S. *Eur. Polym. J.* **2005**, *41*, 231. Park, S. J.; Jin, F. L.; Lee, J. R. *Macromol. Rapid Commun.* **2004**, *25*, 724.

(6) Kim, M. S.; Lee, K. W.; Endo, T.; Lee, S. B. *Macromolecules* **2004**, *37*, 5830.

(7) Khot, S. N.; La Scala, J. J.; Can, E.; Morye, S. S.; Williams, G. I.; Palmese, G. R.; Kusefoglu, S. H.; Wool, R. P. *J. Appl. Polym. Sci.* **2001**, *82*, 703.

(8) Sanchez, C.; Soler-Illia, G. J. de A. A.; Ribot, F.; Lalot, T.; Mayer, C. R.; Cabuil, V. *Chem. Mater.* **2001**, *13*, 3061.

(9) Williams, G. I.; Wool, R. P. *Appl. Compos. Mater.* **2000**, *7*, 421.

(10) Wold, C. R.; Soucek, M. D. *Macromol. Chem. Phys.* **2000**, *201*, 382. Deffar, D.; Teng, G.; Soucek, M. D. *Macromol. Mater. Eng.* **2001**, *286*, 204.

(11) Lligadas, G.; Callau, L.; Ronda, J. C.; Galià, M.; Càdiz, V. *J. Polym. Sci., Part A: Polym. Chem.* **2005**, *43*, 6295.

(12) Thielemans, W.; McAninch, I. M.; Barron, V.; Blau, W. J.; Wool, R. P. *J. Appl. Polym. Sci.* **2005**, *98*, 1325.

(13) Uyama, H.; Kuwabara, M.; Tsujimoto, T.; Nakano, M.; Usuki, A.; Kobayashi, S. *Chem. Mater.* **2003**, *15*, 2492.

(14) Uyama, H.; Kuwabara, M.; Tsujimoto, T.; Nakano, M.; Usuki, A.; Kobayashi, S. *Macromol. Biosci.* **2004**, *4*, 354.

(15) Lu, J.; Hong, C. K.; Wool, R. P. *J. Polym. Sci., Part B: Polym. Phys.* **2004**, *42*, 1441.

(16) Tsujimoto, T.; Uyama, H.; Kobayashi, S. *Macromol. Rapid Commun.* **2003**, *24*, 12. Ballard, R. L.; Tuman, S. J.; Fouquette, D. J.; Stegmiller, W.; Soucek, M. D. *Chem. Mater.* **1999**, *11*, 726.

(17) Vizet, S.; Galy, J.; Gérard, J-F. *Macromolecules* **2006**, *39*, 2574. Castelvetro, V.; Ciardelli, F.; De Vita, C.; Puppo, A. *Macromol. Rapid Commun.* **2006**, *27*, 619. Lin, H. C.; Kuo, S. W.; Huang, C. F.; Chang, F. C. *Macromol. Rapid Commun.* **2006**, *27*, 537. Lee, Y. J.; Huang, J. M.; Kuo, S. W.; Chen, J. K.; Chang, F. C. *Polymer* **2005**, *46*, 2320. Chen, Q.; Xu, R.; Zhang, J.; Yu, D. *Macromol. Rapid Commun.* **2005**, *26*, 1878. Phillips, S. H.; Haddad, T. S.; Tomczak, S. J. *Curr. Opin. Solid State Mater. Sci.* **2004**, *8*, 21. Zheng, L.; Kasi, R. M.; Farris, R. J.; Coughlin, E. B. *J. Polym. Sci., Part A: Polym. Chem.* **2002**, *40*, 885. Pittman, C. U.; Ni, H.; Wang, L.; Li, G. *J. Inorg. Organomet. Polym.* **2001**, *11*, 123. Pyun, J.; Matyjaszewski, K. *Macromolecules* **2000**, *33*, 217. Bharadwaj, B. K.; Berry, R. J.; Farmer, B. L. *Polymer* **2000**, *41*, 7209.

(18) Matejka, L.; Strachota, A.; Pledtil, J.; Whelan, P.; Steinhart, M.; Slouf, M. *Macromolecules* **2004**, *37*, 9449. Abad, M. J.; Barral, L.; Fasce, D. P.; Williams, R. J. *Macromolecules* **2003**, *36*, 3128.

(19) Lee, A.; Lichtenhan, J. D. *Macromolecules* **1998**, *31*, 4970.

(20) Liu, Y. L.; Chang, G. P.; Hsu, K. Y.; Chang, F. C. *J. Polym. Sci., Part A: Polym. Chem.* **2006**, *44*, 3825. Liu, Y.; Zheng, S.; Nie, K. *Polymer* **2005**, *46*, 12016.

(21) Xu, H. Y.; Kuo, S. W.; Lee, J. Y.; Chang, F. C. *Polymer* **2002**, *43*, 5117.

(22) Pellice, S. A.; Fasce, D. P.; Williams, R. J. *J. Polym. Sci., Part B: Polym. Phys.* **2003**, *41*, 1451.

(23) Philips, S. H.; Gonzalez, R. I.; Chaffee, K. P.; Haddad, T. S.; Hoflund, G. B.; Hsiao, B. S.; Fu, B. X. *SAMPE* **2000**, *45*, 1921.

(24) Huang, J. C.; He, C. B.; Xiao, Y.; Mya, K. Y.; Dai, J.; Siow, Y. P. *Polymer* **2003**, *44*, 4491.

(25) Fu, B. X.; Namani, M.; Lee, A. *Polymer* **2003**, *44*, 7739.

(26) Findley, T. W.; Swern, D.; Scalan, J. T. *J. Am. Chem. Soc.* **1945**, *67*, 412.

(27) Rangarajan, B.; Havey, A.; Grulke, E. A.; Culnan, P. D. *J. Am. Oil Chem. Soc.* **1995**, *72*, 1161.

(28) Petrovic, Z.; Zhang, W.; Javni, I. *Biomacromolecules* **2005**, *6*, 713.

(29) Li, G. Z.; Cho, H.; Wang, L.; Toghiani, H.; Pittman, C. U. *J. Polym. Sci., Part A: Polym. Chem.* **2005**, *43*, 355.

(30) Liu, H.; Zheng, S. *Macromol. Rapid Commun.* **2005**, *26*, 196.

(31) Choi, J.; Harcup, J.; Yee, A. F.; Zhu, Q.; Laine, R. M. *J. Am. Chem. Soc.* **2001**, *123*, 11420. Choi, J.; Kim, S. G.; Laine, R. M. *Macromolecules* **2004**, *37*, 99.

BM060703U